

# The variability of orientation maps in cat visual cortex

Matthias Kaschube<sup>1</sup>, Fred Wolf<sup>1</sup>, Theo Geisel<sup>1</sup> and Siegrid Löwel<sup>2</sup>

<sup>1</sup> Max-Planck-Institut für Strömungsforschung, D-37018 Göttingen, Germany.

<sup>2</sup> Leibniz-Institut für Neurobiologie, D-39118 Magdeburg, Germany.

{matze,fred,geisel}@chaos.gwdg.de, loewel@ifn-magdeburg.de

## Abstract

In the visual cortex, orientation domains are arranged in complex patterns. Although several experimental results are consistent with the hypothesis that during development the patterns emerge spontaneously by activity-dependent self-organisation, an innate predetermination of the patterns cannot be ruled out at present. If the pattern-layout is controlled by genetic factors, the patterns observed in pairs of genetically related individuals are expected to be more similar than in genetically unrelated individuals. A necessary prerequisite for evaluating the degree of similarity or dissimilarity between patterns is the quantitative characterisation of their overall interindividual variability. In the present study, we quantitatively analysed the variability of 2-deoxyglucose (2-DG) labelled patterns of orientation domains in area 17 of cat visual cortex. We calculated wavelengths, correlation-lengths, anisotropy parameters and band-parallelism parameters of patterns within the entire area 17 and analysed their statistical relationships. Our results indicate that these parameters are statistically independent. They describe independent aspects of the layout of orientation domains. Furthermore a wavelet analysis showed that local wavelengths were rather constant, whereas the local orientation of band-like 2-DG domains varied across area 17. Taken together, these analyses identify sensitive quantitative indicators for the overall similarity of cortical orientation maps.



Figure 1: [<sup>14</sup>C]2-DG labelled orientation domains in area 17 of cat visual cortex. Autoradiographic labeling is coded in grey scale. Dark regions correspond to domains activated by moving whole-field square wave grating stimuli of one orientation. The boundary of area 17 is indicated by the white line. Scale bar, 1cm.

## 1 Introduction

In the visual cortex, orientation domains are arranged in complex patterns. These patterns differ systematically between species [1,2] and also show considerable interindividual variability [3,4]. Although several experimental results are consistent with the hypothesis that during development the patterns emerge spontaneously by activity-dependent self-organisation (see e.g.

[5,6,7]), an innate predetermination of the patterns cannot be ruled out at present [8]. In principle, the interindividual variability of the patterns is expected to provide important information about the role of innate factors in determining the pattern-layout. If the pattern-layout is controlled by genetic factors, then the patterns observed in pairs of genetically related individuals are expected to be more similar than in genetically unrelated individuals. A necessary prerequisite for evaluating the degree of similarity or dissimilarity between patterns is the quantitative characterisation of their overall interindividual variability. In the present study, we quantitatively analysed the variability of patterns of orientation domains in area 17 of cat visual cortex. Our results identify sensitive quantitative indicators for the overall similarity of cortical orientation maps. In previous studies the wavelength was used to quantify the variability of orientation patterns [9]. In the present study we show that the wavelength vary little compared to other parameters, which appeared to be more appropriate in evaluating the degree of similarity between orientation patterns.

## 2 Methods

We analysed patterns of orientation domains activated by moving whole-field square wave grating stimuli of one orientation. The patterns were obtained by [ $^{14}\text{C}$ ]2-deoxyglucose (2-DG) autoradiography of large flat-mounts of visual cortex. Visual cortical flat-mounts were previously prepared from 31 hemispheres of adult cats [10,3,11]. The 2-DG patterns represent the layout of activated orientation domains within the entire area 17. Figure 1 shows one example. The autoradiographs were first digitised by scanning them with an effective resolution of 18.9 dots per mm cortex using 256 grey-values per dot. For every autoradiograph a region of interest covering area 17 was defined.

In all investigated hemispheres, the orientation domains form regularly spaced patches exhibiting a preference to be organised in bands. In the centre region of the area, the bands are preferentially oriented in parallel to the cortical representation of the horizontal meridian. The precise orientation of the bands is not constant and

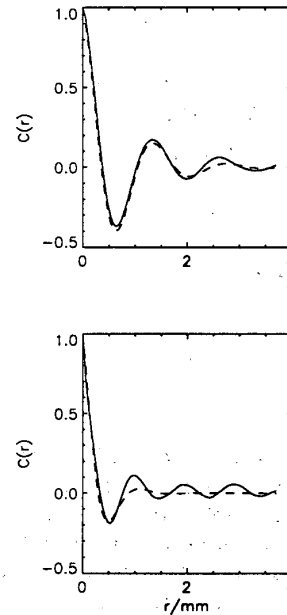


Figure 2: Correlation functions  $C(r)$  for two 2-DG patterns. The solid lines represent the calculated functions; the broken lines represent the fitted functions.

varies systematically in different regions within area 17. There are also regions where the patterns appear rather isotropic and lack a band-like organisation. We used various methods to analyse global and local properties of the 2-DG patterns: global properties were assessed using correlation functions and power spectra; local properties were assessed by a wavelet analysis. For every pattern the 2-dimensional correlation function

$$C(\mathbf{r}) = \langle I(\mathbf{x}) I(\mathbf{x} + \mathbf{r}) \rangle_{\mathbf{x}}$$

was estimated. Here and in the following  $I(\mathbf{x})$  represents the normalised autoradiographic labeling as a function of position  $\mathbf{x}$  within cortex and  $\langle \cdot \rangle_{\mathbf{x}}$  denotes averaging over the entire area 17. For every pattern the correlation-length  $\lambda$  was estimated by fitting a model function

$$c_M(r) = \cos(2\pi r/\lambda) \exp(-r/\lambda)$$

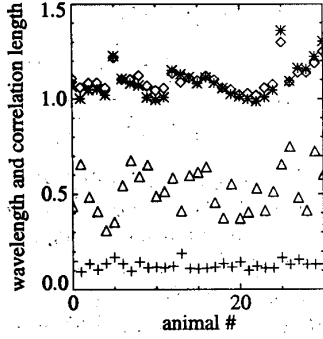


Figure 3: Correlation length  $\lambda$  and wavelength  $\Lambda$  for the 31 investigated patterns. Wavelengths derived from power spectra are represented by diamonds. Wavelengths derived from wavelet transform are represented by the stars. Both methods lead to similar results. Standard deviations of the local wavelengths  $\Lambda(x)$  are given by crosses. Standard deviations appear to be lower than  $0.2mm$ . Correlation lengths are represented by triangles.

to the measured correlation function in the direction maximising  $\lambda$ . The correlation-length  $\lambda$  measures the average regularity of the pattern:  $\lambda$  is proportional to the range over which the positioning of domains can be predicted statistically. We also calculated the power spectra

$$P(\mathbf{k}) = \hat{C}(\mathbf{k})$$

where  $\hat{C}$  denotes the Fourier transform of  $C$ . From  $P$  we estimated the wavelength  $\Lambda$ :

$$\Lambda = 2\pi \left( \frac{\int_0^\infty dk k \int_0^{2\pi} d\theta P(k, \theta)}{\int_0^\infty dk \int_0^{2\pi} d\theta P(k, \theta)} \right)^{-1}$$

The wavelength  $\Lambda$  measures the average distance of adjacent domains preferring similar orientations.

To analyse local properties, a 2-dimensional continuous wavelet transform [12,13] was calculated for every pattern. This transform is given by

$$\tilde{I}(l, \mathbf{x}, \theta) = \int_{\mathbb{R}^2} I(\mathbf{x}') \psi_{l\mathbf{x}\theta}^*(\mathbf{x}') d^2\mathbf{x}' ,$$

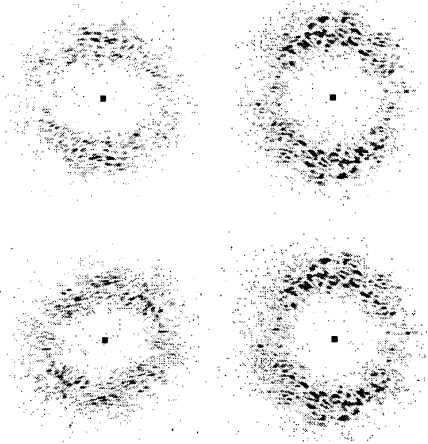


Figure 4: Typical power spectra  $P(\mathbf{k})$  calculated from four different 2-DG patterns. In each power spectrum, the origin of  $\mathbf{k}$ -space is represented by a dot in the centre of the annulus. Grey values code the magnitude of  $P(\mathbf{k})$ . Dark patches represent high magnitude.

where  $\mathbf{x}, \mathbf{x}' \in \mathbb{R}^2$ ,  $\mathbf{x}$  is the position of the wavelet  $\psi_{l\mathbf{x}\theta}$  in cortical coordinates,  $l \in \mathbb{R}_+$  is its scale and  $\theta \in [0, \pi]$  is its orientation.  $\psi_{l\mathbf{x}\theta}$  is defined through a mother wavelet  $\psi(\mathbf{x}')$  by

$$\psi_{l\mathbf{x}\theta}(\mathbf{x}') = \frac{1}{l} \psi \left( \Omega^{-1}(\theta) \frac{\mathbf{x}' - \mathbf{x}}{l} \right)$$

with  $\Omega(\theta)$  being the rotation matrix. For  $\psi(\mathbf{x}')$  to be an admissible mother wavelet it is required that

$$\int_{\mathbb{R}^2} \psi(\mathbf{x}') d^2\mathbf{x}' = 0 .$$

The anisotropy of the pattern suggests the choice of an anisotropic wavelet. We therefore used the anisotropic normalised Morlet wavelet

$$\psi(\mathbf{x}) = e^{i\mathbf{k}_\psi \cdot \mathbf{x}} e^{-\frac{|\mathbf{x}|^2}{2}} ,$$

where  $\mathbf{k}_\psi$  determines the number of oscillations within the Gaussian envelope. From the coefficients  $\tilde{I}(l, \mathbf{x}, \theta)$  we calculated a local scale parameter  $\tilde{l}(\mathbf{x})$  defined as the mean value of  $l$  over

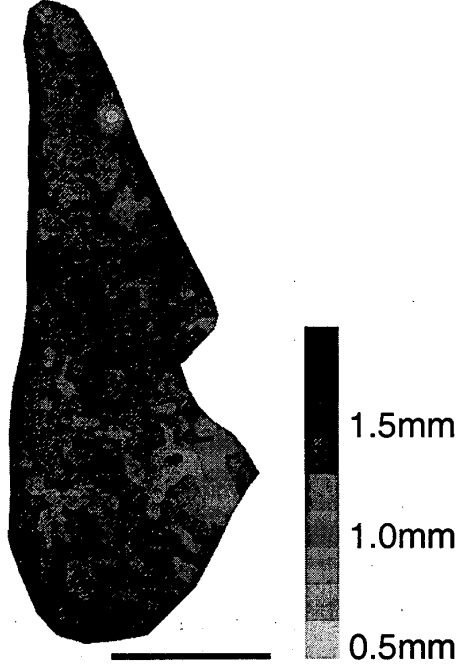


Figure 5: The pattern of local wavelengths  $\Lambda(\mathbf{x})$  of the 2-DG pattern displayed in Figure 1. Local wavelengths are coded in grey scale. Light regions exhibit smaller than average wavelengths. dark regions exhibit larger than average wavelengths. Scale bar, 1cm.

the energy distribution :

$$\bar{l}(\mathbf{x}) = \frac{\int_0^\pi d\theta \int_0^\infty dl \frac{|\bar{I}(l, \mathbf{x}, \theta)|^2}{l^3}}{\int_0^\pi d\theta \int_0^\infty dl \frac{|\bar{I}(l, \mathbf{x}, \theta)|^2}{l^3}},$$

with  $|\bar{I}(l, \mathbf{x}, \theta)|^2/l^3$  being the space-scale energy density.  $\bar{l}(\mathbf{x})$  is the dominant scale at  $\mathbf{x}$ . It therefore determines the wavelength  $\Lambda(\mathbf{x})$  by

$$\Lambda(\mathbf{x}) = \bar{l}(\mathbf{x}) \Lambda_\psi,$$

where  $\Lambda_\psi$  denotes the mean wavelength of the mother wavelet  $\psi$ .

Based on the dominant scale we further calcu-

lated the anisotropy parameter

$$s'(\mathbf{x}) = \frac{\int_0^\pi d\theta |\bar{I}(\mathbf{x}, \theta)|^2 e^{i2\theta}}{\int_0^\pi d\theta |\bar{I}(\mathbf{x}, \theta)|^2}$$

where the dependence of the dominant scale is being suppressed. The factor 2 in the exponent is due to the 180 degree symmetry of the wavelet  $\psi(\mathbf{x})$ . The phase of the complex number  $s'(\mathbf{x}) = |s'(\mathbf{x})| e^{i2\phi(\mathbf{x})}$ ,  $\phi(\mathbf{x})$ , gives the orientation perpendicular to the bands. Its modulus  $|s'(\mathbf{x})|$  is a measure for the anisotropy of the pattern. For an isotropic pattern  $|s'(\mathbf{x})|$  is close to 0, while for a band-like anisotropic structure  $|s'(\mathbf{x})|$  is significantly larger than 0.

Moreover, regions of high  $|s'(\mathbf{x})|$  that exhibit rapid variation in  $\phi(\mathbf{x})$  should also be seen as being isotropic. To account for that  $s'$  was smoothed according to

$$s(\mathbf{x}) = \int_{-\infty}^{\infty} d^2x' s'(\mathbf{x}') K(\mathbf{x}' - \mathbf{x})$$

with  $K$  being the window  $K(\mathbf{x}) = \cos^2(\frac{\pi}{2R}(|\mathbf{x}|)$  for  $|\mathbf{x}| < R$  and  $K(\mathbf{x}) = 0$  else. The radius  $R$  of the filter was typically taken as twice the overall Wavelength  $\Lambda$ .

From  $s(\mathbf{x})$  we calculated the mean anisotropy of the pattern

$$\alpha = \langle |s(\mathbf{x})| \rangle_{\mathbf{x}}$$

and the band-parallelism

$$\nu = \frac{|\langle s(\mathbf{x}) \rangle_{\mathbf{x}}|}{\alpha}$$

### 3 Results

#### 3.1 Global properties of orientation domains

In the visual cortex of cats, the pattern of orientation domains is not isotropic, its anisotropy and the overall variability of the pattern layout can be quantified by correlation functions and power spectra as defined above.

The correlation functions  $C(\mathbf{r})$  were generally anisotropic with the largest correlations occurring parallel to the cortical representation of the

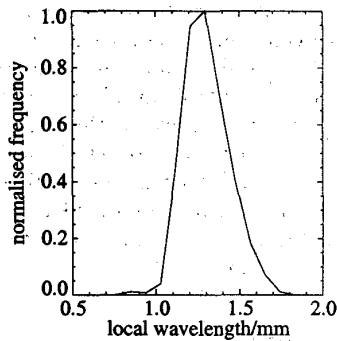


Figure 6: Histogram of the local wavelengths for the 2-DG pattern displayed in Figure 1.

vertical meridian. Figure 2 shows two typical correlation functions, taken as slices of  $C(r)$  in the direction of the smallest overall wavelength. The solid lines represent the measured correlation  $C(r)$ , while the broken lines represent the fitted function  $c_M(r)$ . Positive peaks at  $1\Lambda$ ,  $2\Lambda$  and  $3\Lambda$  are present in the correlation function. Figure 3 shows the wavelengths and their corresponding correlation-lengths for all analysed patterns. Wavelength and correlation-length varied considerably among the patterns. The wavelengths were distributed homogeneously between  $1.0\text{mm}$  and  $1.3\text{mm}$ . The correlation-lengths were distributed homogeneously between  $0.3\text{mm}$  and  $0.8\text{mm}$ .

Typical power spectra  $P(\mathbf{k})$  are displayed in Figure 4. The major contributions to the power spectra are confined to an annulus in wave-vector space. Within this annulus the power  $P(\mathbf{k})$  depends on the direction of the wave-vector. Typically, the largest values were observed for wave-vectors parallel to the cortical representation of the vertical meridian. The smallest values were observed for wave-vectors parallel to the cortical representation of the horizontal meridian. Therefore the anisotropy of  $P(\mathbf{k})$  reflects the preferred orientation of the bands.

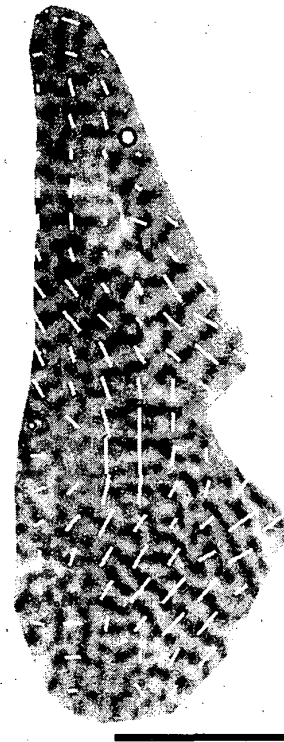


Figure 7: Local anisotropy parameter  $s(\mathbf{x})$  superimposed on the 2-DG pattern. Scale bar,  $1\text{cm}$ .

### 3.2 Local properties of orientation domains

The orientation of the band-like 2-DG pattern is not constant across area 17. The spatial structure of this inhomogeneity was quantified by the local anisotropy parameter  $s(\mathbf{x})$  defined above. The local wavelength  $\Lambda(\mathbf{x})$  was used to demonstrate that the dominant spatial scale of the pattern is rather constant throughout area 17. Figure 5 shows the pattern of local wavelengths for the 2-DG pattern illustrated in Figure 1. Dark regions correspond to larger values, bright regions to lower values.  $\Lambda(\mathbf{x})$  change smoothly over the area thus exhibiting large regions with similar scales. In the pattern of wavelengths, no overall gradient seemed to be present. The corresponding histogram showing the distribu-

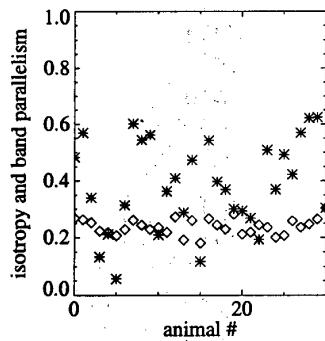


Figure 8:  $\alpha$  and  $\nu$  for the 31 patterns being analysed. The values of  $\alpha$  are represented by the diamonds.  $\nu$  is represented by the stars. Note that the band parallelism  $\nu$  varies substantially among different patterns, whereas the mean anisotropy  $\alpha$  is rather similar.

tion of the wavelengths in the same pattern is illustrated in Figure 6. Figure 7 shows the local anisotropy parameter  $s(x)$  superimposed on the 2-DG labelled orientation domains.  $\phi$  is indicated by the orientation of the bright bars. The lengths of the bars are proportional to  $|s|$ . Within large regions of area 17 the bars have similar size and are oriented parallel to each other indicating the band-like structure of orientation domains in these regions. Figure 8 shows the values of  $\alpha$  and  $\nu$  for all patterns. The anisotropy values were distributed between 0.2 and 0.3. The band-parallelism varied strongly taking values between 0.0 and 0.6.

#### 4 Discussion and Conclusions

We extracted parameters describing quantitatively the layout of patterns of orientation domains. The correlation-length  $\lambda$  and the band-parallelism  $\nu$  varied strongly among the patterns and are therefore likely candidates for sensitive quantitative indicators of similarity and dissimilarity of the patterns. The wavelength  $\Lambda$  and the mean anisotropy  $\alpha$  may also be useful in comparing the patterns. All four parameters

appear to be statistically *independent*. Furthermore our results show that the local wavelengths are rather constant across area 17. In contradistinction, the local orientation (with respect to cortical coordinates) of band-like orientation domains varies within area 17, thus defining subregions in which bands exhibit similar orientations. The spatial organisation of these subregions may provide a more detailed characterisation of the overall layout of the patterns of orientation domains.

#### References

- [1] LeVay, S. and Nelson, S. B. In *Vision and Visual Dysfunction*, chapter 11, 266–315. Macmillan, Houndsmill (1991).
- [2] Wolf, F. and Geisel, T. *Nature* **395**, 73–78 (1998).
- [3] Löwel, S., Bischof, H.-J., Leutenecker, B. and Singer, W. *Exp. Brain Res.* **71**, 33–46 (1988).
- [4] Obermayer, K. and Blasdel, G. G. *J. Neurosci.* **13**, 4114–4129 (1993).
- [5] Ruthazer, E. and Stryker, M. *J. Neurosci.* **16**, 7253–7269 (1996).
- [6] Wolf, F., Bauer, H.-U., Pawelzik, K. and Geisel, T. *Nature* **382**, 306–307 (1996).
- [7] Erwin, E. and Miller, K. D. *J. Neurosci.* **18**, 9870–9895 (1998).
- [8] Hübener, M. *Current Biology* **8**, R342–R345 (1998).
- [9] Obermayer, K. and Blasdel, G.G. *Neural computation* **9**, 555–575 (1997).
- [10] Löwel, S., Freeman, B. and Singer, W. *J. Comp. Neurol.* **255**, 401–415 (1987).
- [11] Löwel, S. and Singer, W. *Dev. Brain Res.* **56**, 99–116 (1990).
- [12] Daubechies, I. *Ten Lectures on Wavelets*, CBMS Lecture Notes Series. SIAM (1991).
- [13] Farge, M. *Annual Review Of Fluid Mechanics* **24**, 395–457 (1992).